Matter and Radiation at Extremes | RESEARCH ARTICLE | scitation.org/journal/mre

# Fuel-ion diffusion in shock-driven inertial confinement fusion implosions

Cite as: Matter Radiat. Extremes 4, 055401 (2019); doi: 10.1063/1.5090783
Submitted: 29 January 2019 • Accepted: 22 May 2019 •
Published Online: 24 July 2019

View Online Export Citation CrossMark

Hong Sio,[1,a)] Chikang Li,[1] Cody E. Parker,[1] Brandon Lahmann,[1] Ari Le,[2] Stefano Atzeni,[3] and Richard D. Petrasso[1]

## AFFILIATIONS

[1] Plasma Science and Fusion Center, Massachusetts Institute of Technology, Cambridge, Massachusetts 02139, USA
[2] Los Alamos National Laboratory, Los Alamos, New Mexico 87545, USA
[3] Dipartimento SBAI, Università degli Studi di Roma "La Sapienza," Via Antonio Scarpa 14, 00161, Roma, Italy

[a)] **Author to whom correspondence should be addressed:** hsio@mit.edu

## ABSTRACT

The impact of fuel-ion diffusion in inertial confinement fusion implosions is assessed using nuclear reaction yield ratios and reaction histories. In $T^3He$-gas-filled (with trace D) shock-driven implosions, the observed $TT/T^3He$ yield ratio is ~2× lower than expected from temperature scaling. In $D^3He$-gas-filled (with trace T) shock-driven implosions, the timing of the $D^3He$ reaction history is ~50 ps earlier than those of the DT reaction histories, and average-ion hydrodynamic simulations cannot reconcile this timing difference. Both experimental observations are consistent with reduced T ions in the burn region as predicted by multi-ion diffusion theory and particle-in-cell simulations.



## I. INTRODUCTION

In inertial confinement fusion (ICF),[1] a spherical target filled with fusion fuel is compressed to reach fusion temperature and density. Conventionally, ICF implosion simulations and modeling rely heavily on average-ion hydrodynamic codes. Understanding the roles of ion kinetics and diffusion has become more important since the start of the National Ignition Campaign[2] in 2009, as highlighted by recent theoretical,[3,4] simulation,[5–7] and experimental[8–12] studies. However, most experimental work has focused on time-integrated measurements, which average over the implosion burn duration and obscure these important effects.

In a hot-spot ignition design, strong shocks are launched into the gas, and the convergence and rebound of these shocks are thought to set up the initial conditions for hot spot formation. These shocks distribute energy to particles proportional to their masses, creating a temperature disequilibrium between the ions and electrons. Because the electrons are more mobile than the ions, they stream ahead and preheat the upstream material. This separation between ions and electrons also creates strong electric fields across the shock front, in addition to the sharp pressure and density gradients. These self-generated electric fields have been observed in ICF implosions,[13] as well as in planar shock-tube[14] experiments.

Recent ICF implosion experiments suggest that kinetic and multi-ion-fluid effects can impact performance in ways not captured by standard hydrodynamic codes such as DUED.[15] These experimentally observed effects include reduced yield,[8] temperature difference between ion species,[9] unexpected yield scaling,[12] ion diffusion,[10] and ion species separation.[11] To address these experimental results, hydrodynamic codes with reduced ion kinetic models[5] and kinetic-ion codes[16] have been used to better capture these multi-ion and kinetic physics in ICF implosions.

In this paper, the impact of ion diffusion in $T^3He$-gas-filled (with trace D) shock-driven implosions and $D^3He$-gas-filled (with trace T) shock-driven implosions is discussed. Section II will outline the experiment and observables. Section III will interpret these data in the context of multi-ion diffusion theory, average-ion hydrodynamic simulations, and particle-in-cell (PIC) simulations. Section IV will discuss future directions and potential implications of these findings.

## II. SHOCK-DRIVEN IMPLOSION EXPERIMENTS

The OMEGA experiments in this work use shock-driven implosions[17] as an experimental platform to probe kinetic and multi-ion effects during shock propagation and rebound in ICF implosions. A shock-driven implosion is one where the bulk of fusion reactions occur from shock heating of the fuel. These simple implosions have been invaluable for studying ICF implosion dynamics because they are low-convergence, 1D in nature, and insensitive to drive asymmetry and hydrodynamic mix.[10] The two sets of implosions described in this work are $T^3He$-gas-filled (with trace D) shock-driven implosions and $D^3He$-gas-filled (with trace T) shock-driven implosions. The spherical targets have an outer diameter of 860 $\mu$m with a ~2.3-$\mu$m-thick $SiO_2$ shell. All 60 laser beams[18] (351 nm, ~14 kJ total, 0.6 ns square pulse shape) are used to illuminate the target. 2D smoothing by spectral dispersion, polarization smoothing, and phase plates are used to improve laser uniformity.

These implosions are hydrodynamiclike, with Knudsen number $N_K \sim 0.3$, estimated here as the ratio of the burn-averaged ion mean free path $\lambda_{ii}$ and the fuel radius $R_{burn}$ at peak nuclear burn. For the $D^3He$-gas-filled (with trace T) implosions, the primary observables are the $D^3He$-p and the DT-n. For the $T^3He$-gas-filled (with trace D) implosions, the primary observables are the $T^3He$-d and the TT-n. The relevant DT, $D^3He$, TT, and $T^3He$ nuclear reactions are

$$\mathrm{D} + \mathrm{T} \rightarrow \alpha(3.5\ \mathrm{MeV}) + \mathbf{n}(\mathbf{14.1\ MeV}), \tag{1}$$

$$\mathrm{D} + {}^3\mathrm{He} \rightarrow \alpha(3.6\ \mathrm{MeV}) + \mathbf{p}(\mathbf{14.7\ MeV}), \tag{2}$$

$$\mathrm{T} + \mathrm{T} \rightarrow \alpha(\leq 6.6\ \mathrm{MeV}) + \mathbf{2n}(\leq \mathbf{10.6\ MeV}), \tag{3}$$

$$\mathrm{T} + {}^3\mathrm{He} \rightarrow \alpha(4.8\ \mathrm{MeV}) + \mathbf{d}(\mathbf{9.5\ MeV})(\mathrm{BR} \sim 43\%). \tag{4}$$

Strong shock heating can potentially cause differences between the ion density profiles (ion diffusion) and/or between the ion temperature profiles (ion thermal decoupling). For example, the T and $^3He$ ion temperatures are expected to be higher than the D ion temperature immediately post shock because of their higher masses. To isolate the mechanism and impact of ion diffusion as far as is reasonably possible, these experiments focus on relatively high gas fill density implosions (>2 mg/cm$^3$), corresponding to a short ion–ion thermalization time (~30 ps) during the shock burn as compared with the burn duration (~100 ps). The second key step taken to reduce the impact of different ion temperatures is to consider reaction pairs where the reactants have the same masses, since collisional shock heating is expected to partition energy to ions according to their masses. For $D^3He$-gas-filled (with trace T) implosions, the reaction pairs DT and $D^3He$ are considered. For $T^3He$-gas-filled (with trace D) implosions, the reaction pairs TT and $T^3He$ are considered. As an example, for two Maxwellian ion populations with two different ion temperatures, the effective fusion temperatures $T_{fusion}$ (for DT and $D^3He$) are given by

$$T_{\mathrm{fusion,D^3He}} = \frac{m_D T_{\mathrm{i,^3He}} + m_{\mathrm{^3He}} T_{\mathrm{i,D}}}{m_D + m_{\mathrm{^3He}}}, \tag{5}$$

$$T_{\mathrm{fusion,DT}} = \frac{m_D T_{\mathrm{i,T}} + m_T T_{\mathrm{i,D}}}{m_D + m_T}. \tag{6}$$

As Eqs. (5) and (6) show, the higher temperatures of $^3He$ and T (resulting from their higher masses) affect the $D^3He$ and DT fusion temperatures in the same way. In general, the fusion reaction yield integrated over the implosion duration for reactants 1 and 2 is given by

$$Y_{12} = \int \frac{f_1 f_2}{1 + \delta_{12}} n_i^2 \langle \sigma v \rangle_{12}\ dV\, dt, \tag{7}$$

where $f$ is the ion species fraction of reactants 1 and 2, $n_i$ is the ion number density, $\langle \sigma v \rangle$ is the Maxwellian-averaged fusion reactivity, and $\delta_{12}$ is the Kronecker delta function. The fusion yield ratio can be approximated as

$$\frac{Y_{11}}{Y_{12}} \approx \frac{1}{2} \frac{f_1}{f_2} \frac{\langle \sigma v \rangle_{11}}{\langle \sigma v \rangle_{12}}. \tag{8}$$

A summary of the main experimental observables is provided in Table I. A suite of optical, nuclear, and X-ray diagnostics are used to diagnose these implosions. For the main experimental observables, the $D^3He$-p and $T^3He$-d yields are measured by wedge-range-filter spectrometers[19] and charged-particle spectrometers.[20] The DT-n yield, the DT temperature, and the TT-n yield are measured by neutron time-of-flight detectors.[21] The nuclear peak emission time (bang time) is measured by the neutron temporal diagnostic.[22]

In Table I, the observed TT/$T^3He$ and DT/$D^3He$ yield ratios have been corrected for the branching ratio in the $T^3He$ reaction, and for the fact that two neutrons are produced per TT reaction. The expected TT/$T^3He$ and DT/$D^3He$ yield ratios are calculated using the fuel fraction and fusion reactivity [Eq. (8)]. The reactivity ratio is a strong function of the ion temperature, and the corresponding expected yield ratio is different for each shot because different ion temperatures are measured on each shot.

Experimentally, the observed yield differences between shots are most likely to have been caused by differences in target shell thickness. For example, shot 86 208 has the thickest shell, latest bang time, highest $T^3He$-d yield, and lowest observed TT/$T^3He$ yield ratio. Laser parameters (total energy and pulse shape) are repeatable to within 3% and are not expected to cause this level of difference. Hydrodynamic simulations also confirm that shell thickness rather than shell diameter has the most direct impact on implosion observables. For both the TT/$T^3He$ and DT/$D^3He$ reaction pairs, the observed yield ratios are lower than the expected yield ratios based on temperature scaling, and interpretations of this observation will be discussed in Sec. III.

In the $D^3He$-gas-filled (with trace T) implosions, DT and $D^3He$ reaction histories are also simultaneously measured with high relative precision (±10 ps) using the particle X-ray temporal diagnostic (PXTD),[23] as shown in Fig. 1. The timing of the $D^3He$ reaction history is ~50 ps earlier than that of the DT reaction history, and this timing differential is much larger than that predicted by average-ion DUED hydrodynamic simulations (~10 ps). As will be discussed in Sec. III, both the observed yield ratios and reaction histories are consistent with the D and $^3He$ ions ahead of the shock front relative to the T ions during shock propagation.

## III. DATA INTEPRETATION

Ion species separation in a multicomponent plasma is driven by sharp pressure and temperature gradients at the shock front and depends on both local plasma conditions (pressure and temperature) and differences in charge and mass between the different ion species.[4] This is a hydrodynamic treatment of multi-ion-species diffusion, which is strictly valid only when the ion–ion mean free path is small compared with the gradient scale lengths. However, as long as the

TABLE I. Summary of primary experimental observables. The uncertainty in the absolute bang time is ±50 ps. The uncertainties in the TT-n, T$^3$He-d, DT-n, and D$^3$He-p yields are ±10%, ±20%, ±5%, and ±20%, respectively. The uncertainty in the DT $T_i$ is ±0.5 keV.

T$^3$He-gas-filled (with trace D) implosions

| Shot | Outer diameter (μm) | $SiO_2$ thickness (μm) | $\rho$ (mg/cm$^3$) | Fraction D | Fraction $^3$He | Fraction T | Bang time (ps) | TT-n yield | T$^3$He-d yield | DT $T_i$ (keV) | TT/T$^3$He (observed) | TT/T$^3$He (expected) |
|---|---|---|---|---|---|---|---|---|---|---|---|---|
| 86 193 | 854 | 2.3 | 2.8 | 0.004 | 0.50 | 0.49 | 780 | $5.3 \times 10^{10}$ | $1.4 \times 10^9$ | 11.7 | 8.0 | 20.0 |
| 86 194 | 853 | 2.4 | 2.8 | 0.004 | 0.50 | 0.50 | 781 | $8.2 \times 10^{10}$ | $1.4 \times 10^9$ | 11.4 | 11.8 | 15.5 |
| 86 195 | 856 | 2.2 | 2.9 | 0.004 | 0.51 | 0.49 | 766 | $7.1 \times 10^{10}$ | $1.4 \times 10^9$ | 11.3 | 10.7 | 22.0 |
| 86 208 | 863 | 2.5 | 3.0 | 0.004 | 0.53 | 0.46 | 837 | $6.5 \times 10^{10}$ | $2.1 \times 10^9$ | 10.5 | 6.5 | 20.0 |

D$^3$He-gas-filled (with trace T) implosions

| Shot | Outer diameter (μm) | $SiO_2$ thickness (μm) | $\rho$ (mg/cm$^3$) | Fraction D | Fraction $^3$He | Fraction T | Bang time (ps) | DT-n yield | D$^3$He-p yield | DT $T_i$ (keV) | DT/D$^3$He (observed) | DT/D$^3$He (expected) |
|---|---|---|---|---|---|---|---|---|---|---|---|---|
| 82 614 | 889 | 2.7 | 2.0 | 0.50 | 0.49 | 0.007 | 841 | $2.0 \times 10^{11}$ | $5.0 \times 10^{10}$ | 11.6 | 4.0 | 5.0 |
| 82 615 | 855 | 2.7 | 2.0 | 0.50 | 0.50 | 0.007 | 831 | $1.9 \times 10^{11}$ | $5.0 \times 10^{10}$ | 10.5 | 3.8 | 6.2 |

plasma is not very kinetic, this treatment does produce qualitatively correct behaviors.

In particular, two diffusion mechanisms play important roles in the interactions between D, $^3$He, and T ions at the shock front, and these mechanisms are driven by the differences in the ion charges and masses. The first mechanism is baro-diffusion, relating to the ion pressure gradient.[3] Baro-diffusion accelerates lighter ions ahead of heavier ions, and will accelerate D ions ahead of T ions. The second mechanism is electro-diffusion, related to the electric potential gradient (the electric field).[4] Electro-diffusion accelerates ions with a higher charge-to-mass ratio ahead of ions with a lower charge-to-mass ratio, and will accelerate $^3$He ions ahead of T ions. In both scenarios, the T ions are behind the D ions and $^3$He ions as the shock propagates inward.

This qualitative picture provided by multi-ion diffusion theory is supported by kinetic-ion PIC LSP[16] simulations, which, in contrast to average-ion hydrodynamic codes, do treat the different ion species separately. In the LSP simulation, the fuel ion species are treated kinetically, while the electrons are treated as a fluid with a flux limiter of 0.06. The choice of flux limiter has been shown to minimally impact LSP results. The simulation uses a 1D spherical geometry with reflecting boundary conditions, with 2000 cells covering a radial distance of 1000 $\mu$m (excluding the origin to avoid numerical stability). The simulation is initialized with 5000 particles per ion species per cell. More information on the PIC simulation setup and collision operators is given in Ref. 7.

Figure 2 illustrates shock propagation in a kinetic-ion LSP simulation that treats the ion populations separately. This simulation is for a D$^3$He-gas-filled (with trace T) implosion. In Fig. 2, as the shock is propagating inward at $t = 0.63$ ns, the D and $^3$He ions are racing ahead. The T ions are notably lagging behind the shock front. This ion species separation at $t = 0.63$ ns during shock convergence developed in a triton depletion in the burn region during shock rebound at $t = 0.73$ ns (when the shock yields are being produced). As expected from the low convergence, mixing of the $SiO_2$ ions into the fuel plasma is negligible in the LSP simulation.

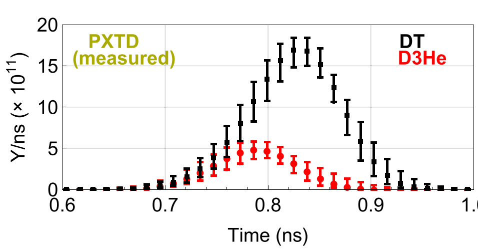


FIG. 1. D$^3$He (red) and DT (black) reaction histories measured on the PXTD in D$^3$He-gas-filled (with trace T) implosions.

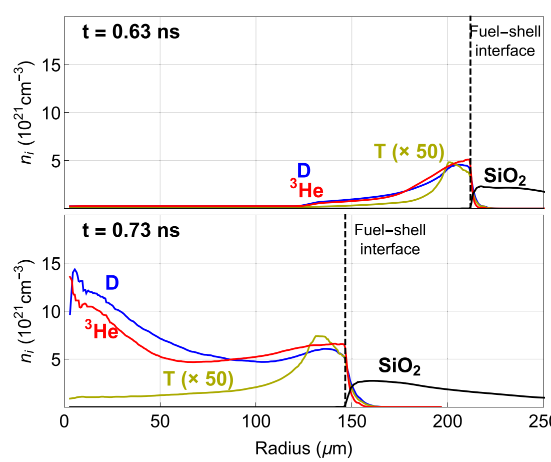


FIG. 2. Density profiles from an LSP simulation of a D$^3$He-gas-filled (with trace T) implosion at $t = 0.63$ ns and $t = 0.73$ ns, during shock convergence and shock rebound, respectively. The ion density profiles for D, T, and $^3$He are in blue, gold, and red, respectively.

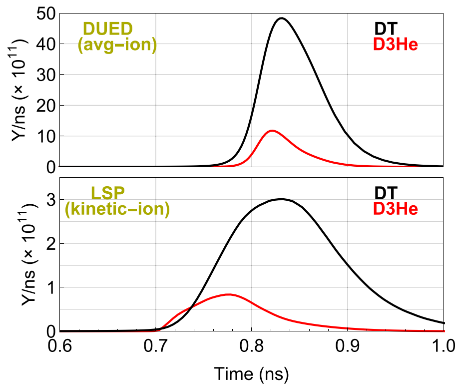


**FIG. 3.** (a) DUED-simulated and (b) LSP-simulated $D^3He$ (red) and DT (black) reaction histories for a $D^3He$ (with trace T) shock-driven implosion.

These differences between the ion density profiles in the kinetic simulation and those in an average-ion-fluid simulation in turn translate to differences in the timing of the simulated reaction histories, which are shown in Fig. 3. In the DUED simulations, the $D^3He$ and DT bang times (the times of peak thermonuclear production) are nearly simultaneous (within 10 ps), which is very different from the measured timing difference and well outside the measurement uncertainty. In contrast, the simulated peak timing difference between the $D^3He$ and DT reaction histories in the kinetic-ion LSP simulation (~50 ps) is in much closer agreement with measurements.

In simulations, the absolute timing and amplitude of the reaction histories (relative to the start of the laser pulse) are strongly affected by many factors (laser energy, absorption, equations of state, flux limiter, etc.). However, the relative timing between the reaction histories is a much more robust and insensitive quantity in the simulation. In the kinetic-ion simulation, the absolute nuclear yield is quite a bit lower than measured, because the laser drive is truncated when the kinetic-ion calculations begin. This has been shown to not affect the relative timing of the simulated reaction histories.

## IV. DISCUSSION AND CONCLUSION

The impact of ion diffusion during the shock phase of ICF implosions has been investigated using both time-integrated and time-resolved nuclear observables. The lower-than-expected $TT/T^3He$ yield ratios (in $T^3He$-gas-filled implosions with trace D) and lower-than-expected $DT/D^3He$ yield ratios (in $D^3He$-gas-filled implosions with trace T) are consistent with tritium depletion in the burn region during shock rebound. At the same time, the observed earlier $D^3He$ reaction history timing relative to that of DT measured using the PXTD and comparison with kinetic-ion simulations provide additional indications that this tritium depletion is related to fuel-ion-species separation that developed during shock propagation into the fuel.

These experimental observations provide new insights into kinetic and multi-ion physics not modeled in average-ion hydrodynamic codes. The experiments here focused on the shock phase of ICF implosions. Using both time-integrated and time-resolved nuclear observables, future experiments will explore these kinetic and multi-ion physics as implosion plasma conditions become increasingly more collisional. Future work will also begin probing how these kinetic and multi-ion effects that developed during the shock phase propagate into and affect hot spot formation during the later compression phase.

## ACKNOWLEDGMENTS

This material is based upon work supported by the Department of Energy, National Nuclear Security Administration under Award Nos. DE-NA0001857, DE-NA0002949, and DENA0002905. The work was also supported in part by NLUF (DE-NA0002035). H.S. was supported by a DOE NNSA SSGF Fellowship (DE-FC52-08NA28752) during this work. S.A. acknowledges Sapienza Project 2016 No. RM11615502006B04, as well as EUROfusion Project Nos. AWP17-ENR-IFE-CEA-01 and ENR-IFE19.CEA-01. A.L. acknowledges the LANL LDRD program. This report was prepared as an account of work sponsored by an agency of the United States Government. Neither the United States Government nor any agency thereof, nor any of their employees, makes any warranty, express or implied, or assumes any legal liability or responsibility for the accuracy, completeness, or usefulness of any information, apparatus, product, or process disclosed, or represents that its use would not infringe privately owned rights. The views and opinions of authors expressed herein do not necessarily state or reflect those of the United States Government or any agency thereof.

## REFERENCES

[1]J. D. Lindl, P. Amendt, R. L. Berger, S. G. Glendinning, S. H. Glenzer *et al.*, "The physics basis for ignition using indirect-drive targets on the National Ignition Facility," Phys. Plasmas **11**, 339 (2004).

[2]J. Lindl, O. Landen, J. Edwards, E. Moses, and NIC Team, "Review of the National Ignition Campaign 2009-2012," Phys. Plasmas **21**, 020501 (2014).

[3]P. Amendt, O. L. Landen, H. F. Robey, C. K. Li, and R. D. Petrasso, "Plasma barodiffusion in inertial-confinement-fusion implosions: Application to observed yield anomalies in thermonuclear fuel mixtures," Phys. Rev. Lett. **105**, 115005 (2010).

[4]G. Kagan and X. Tang, "Electro-diffusion in a plasma with two ion species," Phys. Plasmas **19**, 082709 (2012).

[5]N. M. Hoffman, G. B. Zimmerman, K. Molvig, H. G. Rinderknecht, M. J. Rosenberg *et al.*, "Approximate models for the ion-kinetic regime in inertial-confinement-fusion capsule implosions," Phys. Plasmas **22**, 052707 (2015).

[6]C. Bellei, P. A. Amendt, S. C. Wilks, M. G. Haines, D. T. Casey *et al.*, "Species separation in inertial confinement fusion fuels," Phys. Plasmas **20**, 012701 (2013).

[7]A. Le, T. J. T. Kwan, M. J. Schmitt, H. W. Herrmann, and S. H. Batha, "Simulation and assessment of ion kinetic effects in a direct-drive capsule implosion experiment," Phys. Plasmas **23**, 102705 (2016).

[8]M. J. Rosenberg, H. G. Rinderknecht, N. M. Hoffman, P. A. Amendt, S. Atzeni *et al.*, "Exploration of the transition from the hydrodynamiclike to the strongly kinetic regime in shock-driven implosions," Phys. Rev. Lett. **112**, 185001 (2014).

[9]H. G. Rinderknecht, M. J. Rosenberg, C. K. Li, N. M. Hoffman, G. Kagan *et al.*, "Ion thermal decoupling and species separation in shock-driven implosions," Phys. Rev. Lett. **114**, 025001 (2015).

[10]H. G. Rinderknecht, H. Sio, C. K. Li, A. B. Zylstra, M. J. Rosenberg *et al.*, "First observations of nonhydrodynamic mix at the fuel-shell interface in shock-driven inertial confinement implosions," Phys. Rev. Lett. **112**, 135001 (2014).

[11]D. T. Casey, J. A. Frenje, M. Gatu Johnson, M. J.-E. Manuel, H. G. Rinderknecht *et al.*, "Evidence for stratification of deuterium-tritium fuel in inertial confinement fusion implosions," Phys. Rev. Lett. **108**, 075002 (2012).

[12]H. W. Herrmann, J. R. Langenbrunner, J. M. Mack, J. H. Cooley, D. C. Wilson *et al.*, "Anomalous yield reduction in direct-drive deuterium/tritium implosions due to $^3He$ addition," Phys. Plasmas **16**, 056312 (2009).

[13]C. K. Li, F. H. Séguin, J. R. Rygg, J. A. Frenje, M. Manuel *et al.*, "Monoenergetic-proton-radiography measurements of implosion dynamics in direct-drive inertial-confinement fusion," Phys. Rev. Lett. **100**, 225001 (2008).
[14]H. Sio, R. Hua, Y. Ping, C. McGuffey, F. Beg *et al.*, "A broadband proton backlighting platform to probe shock propagation in low-density systems," Rev. Sci. Instrum. **88**, 013503 (2017).
[15]S. Atzeni, A. Schiavia, F. Califanob, F. Cattanib, F. Cornoltib *et al.*, "Fluid and kinetic simulation of inertial confinement fusion plasmas," Comput. Phys. Commun. **169**, 153 (2005).
[16]D. R. Welch, D. V. Rose, R. E. Clark, T. C. Genoni, and T. P. Hughes, "Implementation of an non-iterative implicit electromagnetic field solver for dense plasma simulation," Comput. Phys. Commun. **164**, 183 (2004).
[17]M. D. Rosen and J. H. Nuckolls, "Exploding pusher performance—A theoretical model," Phys. Fluids **22**, 1393 (1979).
[18]T. R. Boehly, D. L. Brown, R. S. Craxton, R. L. Keck, J. P. Knauer *et al.*, "Initial performance results of the OMEGA laser system," Opt. Commun. **133**, 495 (1997).
[19]F. H. Seguin, N. Sinenian, M. Rosenberg, A. Zylstra, M. J.-E. Manuel *et al.*, "Advances in compact proton spectrometers for inertial-confinement fusion and plasma nuclear science," Rev. Sci. Instrum. **83**, 10D908 (2012).
[20]F. H. Séguin, J. A. Frenje, C. K. Li, D. G. Hicks, S. Kurebayashi *et al.*, "Spectrometry of charged particles from inertial-confinement-fusion plasmas," Rev. Sci. Instrum. **74**, 975 (2003).
[21]V. Yu. Glebov, C. J. Forrest, K. L. Marshall, M. Romanofsky, T. C. Sangster *et al.*, "A new neutron time-of-flight detector for fuel-areal-density measurements on OMEGA," Rev. Sci. Instrum. **85**, 11E102 (2014).
[22]C. Stoeckl, R. Boni, F. Ehrne, C. J. Forrest, V. Yu. Glebov *et al.*, "Neutron temporal diagnostic for high-yield deuterium–tritium cryogenic implosions on OMEGA," Rev. Sci. Instrum. **87**, 053501 (2016).
[23]H. Sio, J. A. Frenje, J. Katz, C. Stoeckl, D. Weiner *et al.*, "A Particle X-ray Temporal Diagnostic (PXTD) for studies of kinetic, multi-ion effects, and ion-electron equilibration rates in Inertial Confinement Fusion plasmas at OMEGA (invited)," Rev. Sci. Instrum. **87**, 11D701 (2016).